5A.3 ANALYSES of RADAR ROTATIONAL VELOCITIES and ENVIRONMENTAL PARAMETERS for TORNADIC SUPERCELLS in TROPICAL CYCLONES

Roger Edwards,[1] Bryan T. Smith, Richard L. Thompson, and Andrew R. Dean
Storm Prediction Center, Norman, OK

1. BACKGROUND

For the purposes of forecasting severe local storms, the primary hazard within a tropical cyclone (TC) is the tornado. Climatologically, TC tornadoes generally are smaller, shorter-lived and weaker in terms of damage rating than their midlatitude counterparts (Edwards 2012). Because of the relative distribution and juxtaposition of supportive kinematic and thermodynamic ingredients, TC tornadoes are most commonly found over a sector north through east and southeast of center (e.g., McCaul 1991; Schultz and Cecil 2009; Edwards 2012).

Ingredients-based thinking (e.g., Johns and Doswell 1992) has become a crucial foundation for severe-storms forecasting, and this includes TC tornadoes. Most TC tornadoes are supercellular in origin as evident in radar analyses (Edwards et al. 2012a, hereafter E12a), and nonsupercellular TC tornadoes tend to occur in association with environmental conditions similar in magnitude to those with supercells (Edwards et al. 2012b). However, TC tornadoes as a whole generally develop in environments characterized by weaker lapse rates, smaller CAPE, greater moisture and larger measures of lower-tropospheric wind shear than those spawned by nontropical processes (McCaul 1991; E12a).

Radar characteristics of tornadic storms, including reflectivity patterns, rotational velocity (hereafter V_{rot}), and echo depth, can be used to infer environmental conditions. This includes information that otherwise may not be available to the operational forecaster because of limitations in the density of in situ observations (surface stations, rawinsonde releases, aircraft soundings, etc.) and/or the capability of automated mesoanalyses to depict the parameters accurately. As an extreme example, if radar output depicts an intense mesocyclone within a discrete cell bearing a collocated reflectivity hook echo, especially with scan-to-scan temporal continuity, forecaster confidence is high that 1) a supercell is present, and by extension, 2) enough lift, moisture, vertical shear, and instability exist to support a supercell, regardless of any available environmental data to the contrary. Ideally, radar and other analytic and diagnostic input do not conflict substantially, but instead, synergize to offer the forecaster a conceptual model of the situation that is more complete than that obtained solely from one source.

To that end, this study extends a prolonged project to examine storm modes and environmental parameters for severe-storm reports (Smith et al. 2012; Thompson et al. 2012), relate damage rating to environmental and radar characteristics (Smith et al. 2015), and all of the above for a subset of TC tornadoes in particular (E12a and this work). Section 2 documents the data and analytic techniques used. Section 3 presents our preliminary results, and section 4 offers some conclusions and discussion.

2. DATA and METHODS

We analyze the environments and radar characteristics accompanying TC tornadoes using a combination of:

- A 2010–2014 subset of the Storm Prediction Center (SPC) TC tornado records (TCTOR; Edwards 2010);
- An environmental dataset composed of hourly, gridded, three-dimensional mesoanalysis fields (Schneider and Dean 2008);
- Operationally implemented "super-resolution" (Torres and Curtis 2007) WSR-88D data.

More details follow on each source, respectively, with emphasis on the radar aspects given the nature of this conference. Smith et al. (2014) offer additional discussion on the development of the SPC tornadic storm and environment data.

a. Events

The number of tornadic events examined here (112 supercellular, four others) differs from the total TC tornado tally for the period (139). This is related to two factors: 1) county segments are used here, whereas TCTOR is whole-tornado-based, and 2) our use of the gridded report-filtering scheme detailed in Smith et al. (2012) that keeps only the highest rated tornado when more than one appear in a 40-km grid square. For our purposes, as in E12a, a "tornado" is that county-segment of a recorded tornado path assigned the highest rating on the Enhanced Fujita (EF) scale (WSEC 2004; Edwards et al. 2013). Of the 112 supercellular events, 26 (23%) needed radar-based time adjustment, compared to 7% of 730 events in the E12a dataset. See E12a, section 3a, for more complete discussion of the nature of report-time errors for TC tornadoes.

[1] *Corresponding author address:* Roger Edwards, Storm Prediction Center, National Weather Center, 120 Boren Blvd #2300, Norman, OK 73072; E-mail: roger.edwards@noaa.gov

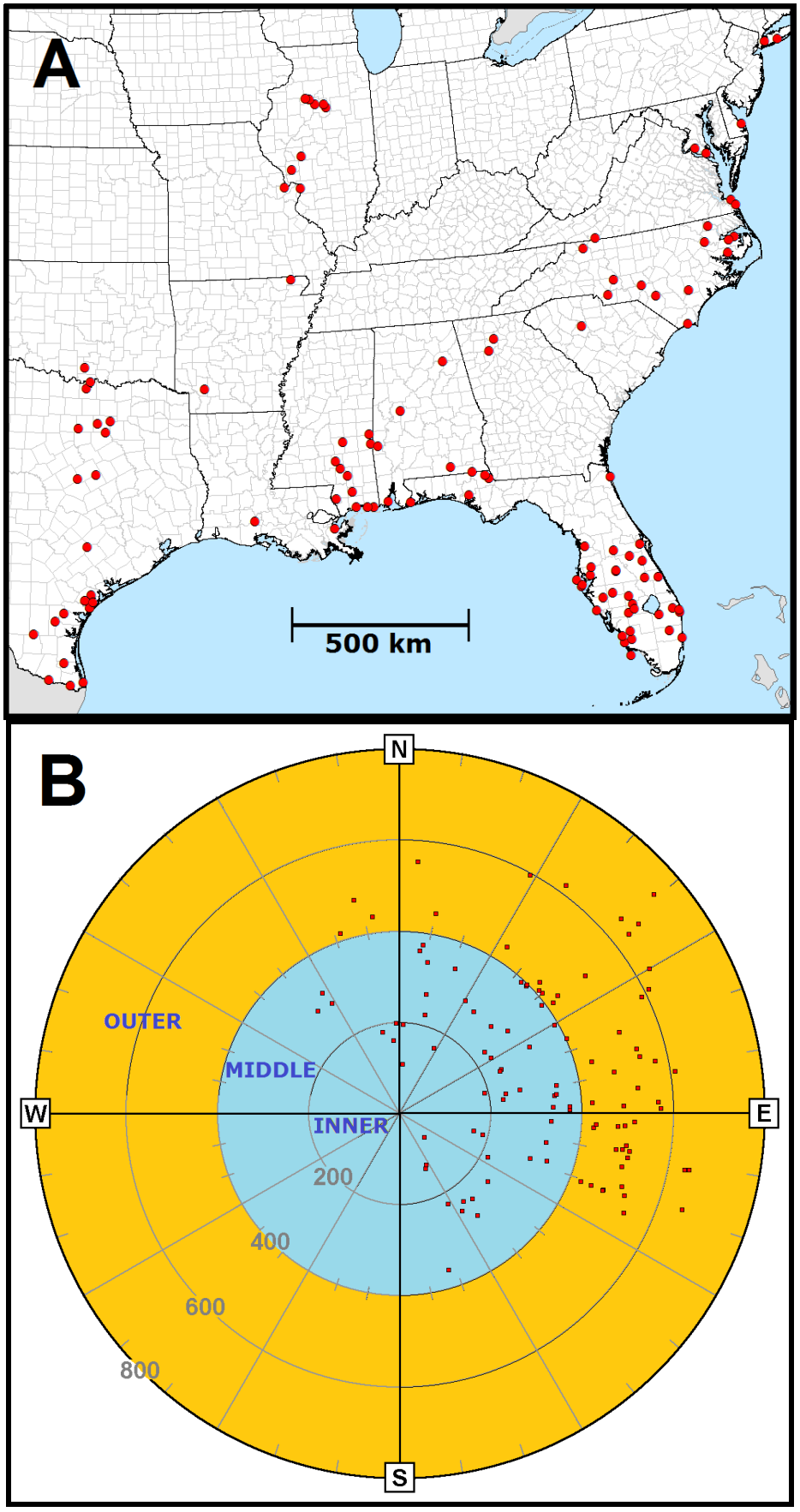

Figure 1: Locations of tornado events studied (red dots) with respect to: a) central and eastern U.S. geography and b) azimuth (radials every 30°) and range (km, as labeled) from TC center. Outer (400–800 km) and combined inner (0–199 km) and middle (200–399 km) sectors labeled and colored. Some proximal events may obscure each other.

Otherwise, methods for gridding and sorting the environmental dataset, selecting storm events, and matching the two datasets spatiotemporally with grid-box filtering, also followed Smith et al. (2012) in general and E12a for TC tornadoes. Specifically, the same environmental variables and parameters are used in this study. Tornado events included here are mapped in Fig. 1, both geographically and with respect to TC center at tornado time (the latter taken from TCTOR).

The TC-relative distribution of tornadoes herein closely matches that of tropical storms in the TCTOR dataset (e.g., Fig. 6c in Edwards 2012), but lacks events at 400–800-km distances southeast of center that are present in the data for all TC intensity categories in prior years. Any attempt to explain this slight but noticeable sectoral deviation from the larger climatology would be speculative and outside the scope of our analysis.

Events were constrained to be within 101 mi (163 km) of radar sites owing to beam-height sampling considerations at greater distances. For this study, emphasis was placed on supercells and marginal supercells, since only four non-supercellular TC tornadoes (Edwards et al. 2012b) were found, and no tornadoes with other modes associated with midlatitude events in Smith et al. (2012, 2015). For brevity, "tornado" stands for ""tornadic event" hereafter.

b. Radar

For radar data, the "super-resolution" approach accomplishes 0.5° azimuthal spacing along 250-m range resolution via oversampling in the scanning strategy (Brown et al. 2002, 2005; Torres and Curtis 2007). Much more of this data is now available for study than in E12a; in fact, our current study period (below) entirely falls within the "super-resolution" timeframe that began in summer 2008. Nonetheless, sample-size concerns are valid given that the period of availability of "super-resolution" data and especially dual-polarimetric data from the WSR-88D network corresponds to a marked dearth in landfalling TCs in the U.S., an absolute absence of major (category 3 or higher) hurricane landfalls that tend to produce large numbers of tornadoes per storm (Edwards 2012), and a resulting relative lull in overall TC tornado occurrence, compared to the mid-2000s.

The 0.5°-beam V_{rot} was logged for each case event, using the methodology detailed in Smith et al. (2015). To summarize: after assigning convective mode to the start time of a tornadic event via WSR-88d image interrogation, peak V_{rot} during tornado lifespan was determined manually using radial-velocity imagery pulled from NCDC digital inventory and displayed in Gibson Ridge Level II Analyst software.

After Edwards et al. (2012b, e.g., their Fig. 8), a 20-dB*Z* echo top (ET) was recorded for the volume scan closest to adjusted tornado time for each event, using the nearest WSR-88D unit for which storm-depth information was available. Similarly, we used horizontally sliding, vertical range-height indicator (RHI)-style cross-sections through each tornadic echo. However, this time, instead of rounding to the nearest 1000 ft (305 m), we interpolated linearly between elevation angles straddling the top of the chosen reflectivity value. This follows the newer RHI-based ET approach recommended by Lakshmanan et al. (2013). The ET threshold here was kept at 20 dB*Z*, since:

- This value is consistent with the criteria for tropical convection established in Cifelli et al. (2007); and
- It is the closest RHI contour value in GRLevel2™ software to the 18-dB*Z* midlatitude convention exemplified by Lakshmanan et al. (2013).

In addition, dual-polarimetric capabilities (Bringi and Chandrasekar 2001) became part of the operational NWS radar-data stream beginning in November 2010 (NWS 2010). In particular, appearances of mesocyclone-collocated, beam-planar anomalies and vertically continuous columns of relatively low copolar cross-correlation coefficient (ρ_{hv}), with values substantially less than one, tend to indicate lofted tornadic debris fields (Rhyzhkov et al. 2005). The tornadic debris signature (TDS) is a somewhat time-lagged diagnostic and not prognostic tool, given the need for debris to be advected vertically to detectable levels. Nonetheless, low-ρ_{hv} anomalies have been related to severity of damage for nontropical, supercellular tornadoes (Bodine et al. 2013).

Given such utility, and the dearth of TC tornado-related TDS documentation, ρ_{hv} also has been recorded for each case in this study where dual-polarimetric data were available, beginning with TC Irene in North Carolina, 27 August 2011. Tornadic debris signatures (TDS) were evident in 23 cases. Analyses of ρ_{hv} data were not included in E12a due to a small number of cases then, but are investigated here. Consistent with NWS Warning Decision Training Branch (2015) guidelines, we use ρ_{hv} values of ≤0.95 and/or a local minimum, collocated with reflectivity 20 dB*Z*. For methodological consistency, TDS top was determined using the aforementioned echo-top technique of Lakshmanan et al. (2013), but applied to the highest beam level of the ρ_{hv} plume apparent in RHI cross sections that was vertically continuous with the underlying TDS (if more than the lowest beam contained a ρ_{HV} minimum).

Figures 2 and 3 show a case example with three base moments[2] and ρ_{hv} using along-beam and vertical planes, all conterminous. Assessing vertical and lateral extent of a TDS necessarily was subjective given inherent beam-resolution limitations and the commonly noisy nature of ρ_{hv} aloft (e.g., Fig. 3a). Still, in the deeply warm-cloud TC setting, where

[2] Though specific values of base reflectivity and spectrum width were not tabulated for this work, imagery of each moment assisted in subjectively identifying and tracking tornadic echoes; see Spoden et al. (2012) for discussion on this and other utilities of spectrum width.

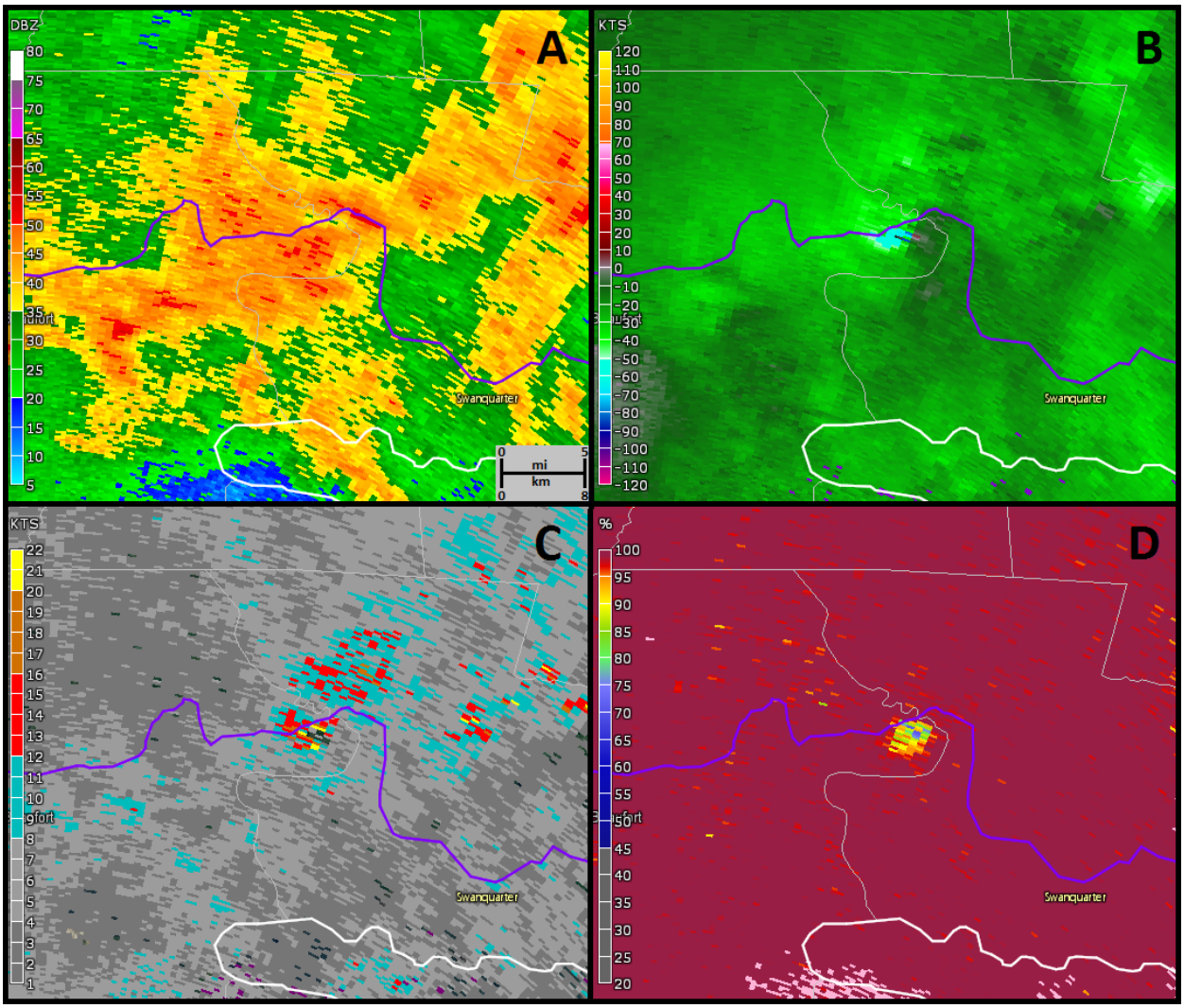

Figure 2: Morehead City, NC WSR-88D products at 0.5° elevation angle, 0203 UTC 27 August 2011, for an EF1 tornado (located near center of each panel): a) base reflectivity, b) base velocity, c) spectrum width, d) ρ_{HV}. Values and units as shown in scales. Tornado was in extreme eastern Beaufort County, NC at this time, northwest of Swanquarter, moving generally westward (right–left). Purple curve is U.S. Highway 264.

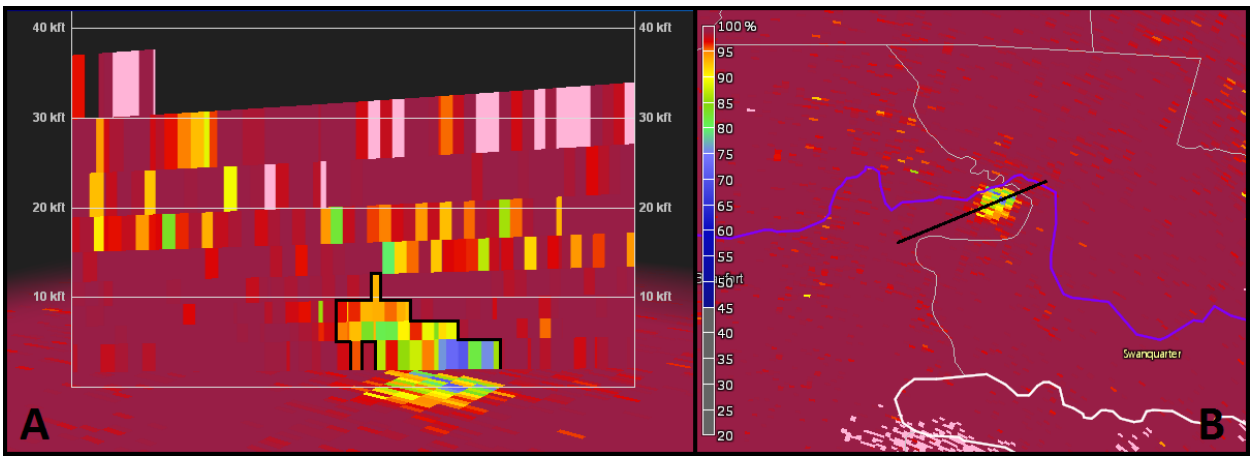

Figure 3: a) RHI Cross section through the ρ_{HV} min depicted in Fig. 1d, from left to right along the black line shown in panel (b). Black outline in (a) represents approximate bounds of the TDS using ρ_{hv} ≤0.9.

warm-rain processes dominate cell depth, hail is rare to nonexistent in low levels, and mixed-phase regions are relatively high aloft, TDS-associated ρ_{hv} minima hypothetically should be obvious. In most cases they were, especially at 0.5° beam elevation.

3. RESULTS and CONCLUSIONS

Unlike in E12a, the full set of environmental data described in Thompson et al. (2012) was available for each case—albeit for a considerably smaller sample size (112 events associated supercell and marginal supercell modes here compared to 639 in E12a). As for new analyses not in E12a, ET and V_{rot} were determined for all cases, and anomalous ρ_{hv} found in 23 tornadoes. Environmental, V_{rot} and ET data were examined for the following damage-rating, convective-mode and spatiotemporal categories: all rated EF0, all rated ≥EF1, non-marginal supercellular EF0, all non-marginal supercells, marginal supercells, all events, all daytime (1200 UTC to 2359 UTC, following Edwards 2012) and nighttime (0000-1159 UTC), and inner-middle (<200 km from TC center) versus outer (≥200 km). Sample-size considerations preclude more precise breakdowns until more events are accumulated in the super-resolution, dual-polarized radar era. This includes distinctions between weak (EF0–EF1) and strong (EF2–EF3) events, because of the lack of the latter in this dataset so far (5 and 0, respectively). Instead, EF1 and EF2 events were grouped for analyses. As in E12a, before performing analyses, errors in the data were found and corrected.

a. Error sources in tornado data

As in E12a, the most common errors were temporal mismatches between the tornado report times and associated radar signatures (via reflectivity). Such adjustments were made in 26 cases (23% of the data), compared to just 7% of the events in E12a. The average absolute time error was 21 min with extrema of 2 and 167 min. Twenty-two (85%) of time errors were positive (i.e., the times had to be adjusted backward). Even when discounting six cases adjusted at least in part due to strong ρ_{hv} (TDS) evidence (which wasn't available for E12a), the overall percent of cases that needed time adjustment is considerably higher here. As such, we have no non-speculative explanation for the larger number of report times needing correction here versus in E12a. Only two time adjustments were precisely 60 min, indicating less of a time-zone-translation problem than evident in pre-processed E12a data (where associated 1-h errors were the most common type).

In two cases *not included* in the aforementioned temporal corrections, the time recorded for this analysis differed from TCTOR report time due to the use of the second county-segment of a multi-county tornado. Those also are not included in the error computations above. One of the two cases (on 4 September 2011) also involved a state-border crossing of a tornado from Florida into Alabama, which required use of the latter segment.

Obvious location errors were rare. In one case the decimal digits of the latitude, when transposed from those in *Storm Data*, matched the tornado location. In four of the six ρ_{hv}–adjustment cases, TDS signatures began at least one volume scan before the time and location of the tornado report. Those tornado starts were adjusted conservatively to the scan time and estimated location, though they almost certainly began an unknown time and distance prior.

b. Environmental analyses

With respect to storm modes and tornado ratings, very little separation in distributions appeared among most thermodynamic parameters tested, such as 100-hPa mean-mixed-layer (ML) CAPE (Fig. 4), surface-based (SB) CAPE, 0–3-km AGL CAPE, various layer samplings of lapse rate and PW (not shown). Most CAPE measures and lapse rates showed slight distinction between EF0 and ≥EF1 events (e.g., Figs. 4 and 5). The 700–500-hPa lapse rates exhibited the greatest separation with respect to tornado rating among thermodynamic parameters, with EF1–EF3 tornadoes about a quartile lower than EF0 events and marginal supercells nearly a quartile higher than full supercells. By contrast, 850–500-hPa lapse rates (not shown) were much more indistinct across all categories.

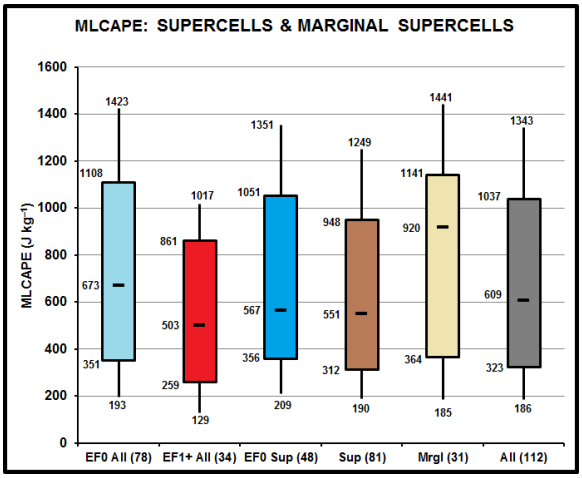

Figure 4: Box plots of 100-hPa MLCAPE (J kg^{-1}) for (left–right) EF0 tornadoes (cyan), ≥EF1 (red), supercellular EF0 (blue), all supercells (light brown), marginal supercells (cream), and all events (gray). Boxes encompass 25th–75th percentiles around the median (bar) with values alongside. Whiskers extend to 10th and 90th percentiles with values off ends. Sample sizes given in parentheses.

Thermodynamic parameters also generally showed very little distinction between daytime and nighttime across all events, except for low-level lapse rate (Fig. 6). This result is consistent with the diurnal heating cycle. However, MLCAPE and 0–3-km CAPE each showed substantial overlap between day and night, with daytime upper percentiles extending higher (not shown). This likely attests to the relative homogeneity of the TC environment compared to midlatitude baroclinic waves, with only minor thermal differences (e.g., when subtle boundaries are present, as discussed in Edwards and Pietrycha 2006). Greater dewpoint depressions were evident by day, with very similar relative distributions (not shown) to 0–3-km lapse rates in Fig. 6. This implies that

diabatically driven, diurnal, boundary-layer mixing was the main counterbalancing effect against larger lapse rate for keeping daytime low-level CAPE similar to that at night.

Comparing TC sectors, all thermodynamic variables exhibited strong interquartile overlap, with only slight upward differences in 0–3-km lapse rate and MLCAPE in the outer versus inner 400 km radii from TC center (not shown).

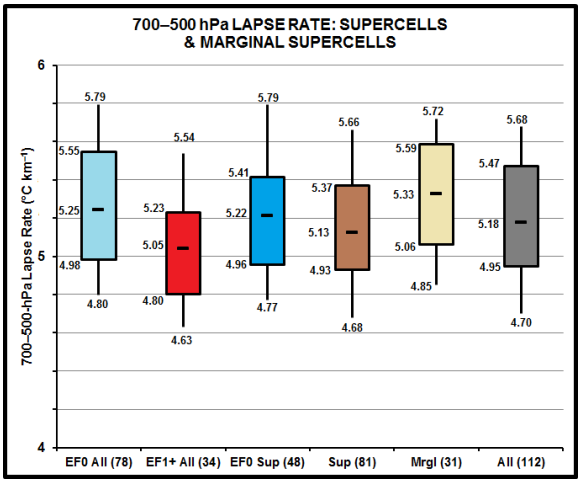

Figure 5: As in Fig. 4, but for 700–500-hPa lapse rate.

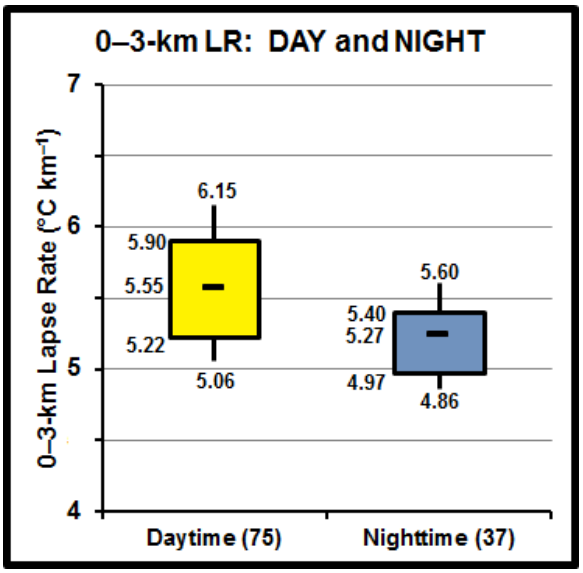

Figure 6: Boxplots of 0–3-km AGL lapse rate (C km^{-1}) by day (yellow) and night (slate blue), as defined in the text. Box and whisker percentiles same as in preceding figures.

Kinematic parameters examined in E12a were analyzed here as well, and similarly exhibited greater distinctions across event classes than thermodynamic measures. These likewise exerted the greater influence on composite indices, versus that of the relatively indistinct thermodynamic variables. Bulk wind difference (BWD) through the 0–1 and 0–6-km layers, 0–1 and 0–3-km storm-relative helicity (SRH), and both BWD and SRH computed from effective-inflow layer methods (Thompson et al. 2007), were greater for ≥EF1 events than EF0, and for supercells versus marginal supercells. Figure 7 illustrates these findings for 0–1-km SRH. Fixed-layer measures showed greater interquartile separation than effective layers, unlike the Thompson et al. (2007) dataset that was composed of non-TC events. This may be related to the lower buoyancy characteristic of TC tornado environments in general, compared to those in midlatitude systems (E12a).

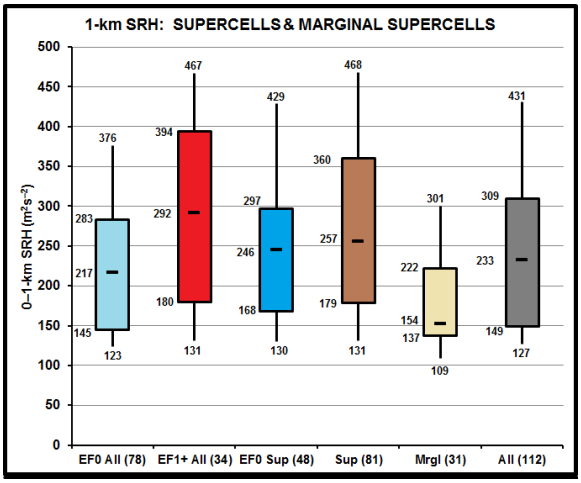

Figure 7: As in Fig. 4, but for 0–1-km BWD (kt).

Assorted measures and indicators of low-level shear showed well-defined distinction from day to night (stronger shear at night; e.g., Fig. 8) and outward with respect to storm center (stronger shear inward; Fig. 9a). These influences were muted in bulk indices such as SCP and STP, however, by the generally strong overlap of CAPE distributions (not shown). Daytime CAPE distributions did extend to larger values than at night, but still with great overlap around the median and lower quartiles. One exception to the weaker outer-sector shear magnitude was with 0–6-km BWD (Fig. 9b). The two radial sectors each contained 56 tornadic supercells, and exhibited similar distributions of SCP and STP (not shown). Since we did not examine nontornadic storms, it is unclear as to whether the larger inner-sector values of 0–1-km SRH mattered in terms of tornadic production rate for supercells.

The combined CAPE and shear parameter-space shape for this dataset (Fig. 10) strongly resembles that of midlatitude climatological scatterplots using various measures of buoyancy and shear (e.g., Fig. 20 in Johns and Doswell 1992). The four TC cases they plotted constituted a very small sample of F2 or greater cases, and were found in the lower left (lower CAPE and shear) part of the parameter space otherwise occupied by EF2+ tornadoes in midlatitude events. Direct comparison of values with their dataset is not straightforward for our 112 cases, however, since the Johns and Doswell (1992) plot differed so much in a multivariate manner, using:

- Only tornadoes rated F2 or stronger,
- Different parcels for CAPE (surface-based instead of 100-hPa mean-mixed layer)
- Different SRH-input layer depth (0–2 km)

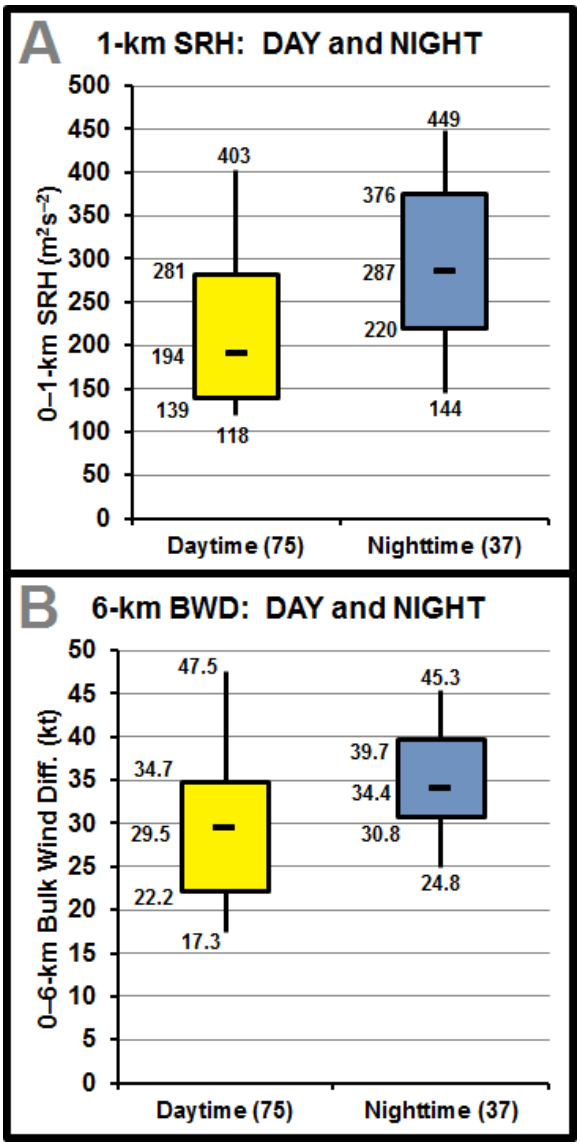

Figure 8: Each panel as in Fig. 6, but for a) 0–1-km SRH and b) 0–6-km BWD.

- Different storm-motion assumption (30 right-deviant, 75% of mean-wind speed, versus Bunkers et al. 2000 "internal dynamics" method here).

c. V_{rot} analyses

Peak rotational velocities were documented for all 112 cases. The mean value was 25.9 kt (13.3 m s^{-1}), with a median of 24.8 kt (12.8 m s^{-1}), a maximum of 59.7 kt (30.7 m s^{-1}) and a minimum of 9.7 kt (5 m s^{-1}). The largest value, associated with an EF1 tornado from TC Debby (0021 UTC 25 June 2012), fit just outside the 75th percentile of EF2-rated supercellular tornadoes nationwide in the Smith et al. (2015) distributions from 2009–13. That event also fell just below the 63-kt (32.4 m s^{-1}) V_{rot} median of their EF3 cases, and within the uppermost reaches of their 50.0–59.9-kt bin that yields a 39% conditional probability of an EF2+ tornado for all convective modes.

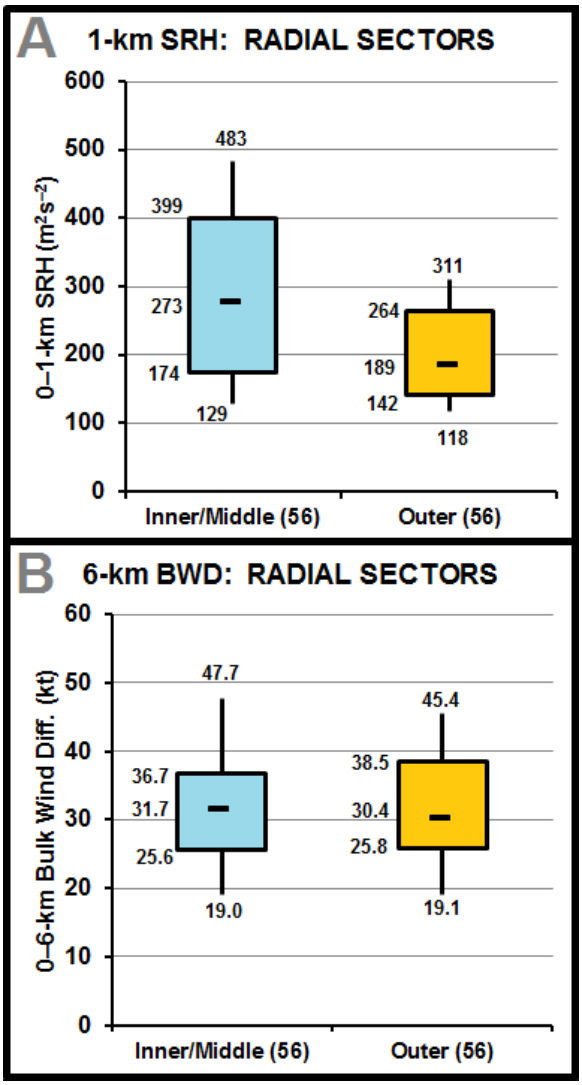

Figure 9: Boxplots for radial sectors as colored on the Fig. 1b polar graph, <200 km from TC center (cyan) and ≥200 km (gold): a) 0–1-km SRH and b) 0–6-km BWD.

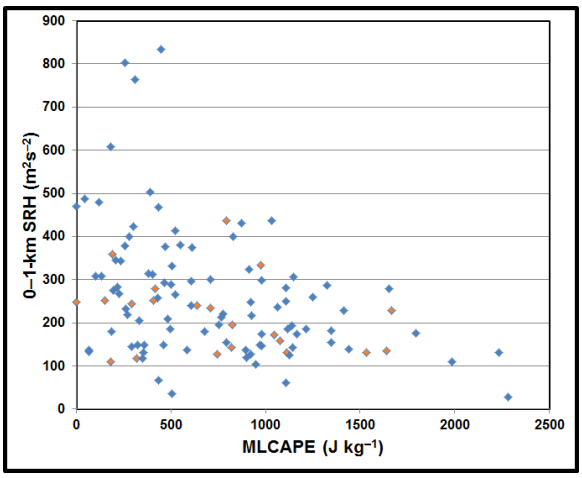

Figure 10: Scatterplot of MLCAPE (abscissa) and 0–1-km SRH (ordinate) for all cases. Those producing TDSs (section 3c) are colored orange.

With a sample size of just five EF2 TC events and no EF3+, meaningful comparisons are difficult to make. Still, the average TC EF2 V_{rot} of 30.4 kt (15.6 m s^{-1}) is 4.5 kt (2.3 m s^{-1}) above that of the dataset as a whole (above). The minimum V_{rot} herein, associated with TC Isaac (1824 UTC 1 September 2012) fell 13 kt (6.7 m s^{-1}) below the 10th percentile for supercellular EF0 tornadoes in the Smith et al. (2015) data, and itself was rated EF0. The median V_{rot} of all TC tornadoes herein fell below the 25th percentile of EF0 supercellular tornadoes nationwide (e.g., their Fig. 3). Any reason for this remains speculative, but may be related to the greater difficulty of resolving mesocyclones and their peak V_{rot} associated with tornadic TC supercells that tend to be smaller, shallower and shorter-lived than their midlatitude counterparts (Edwards 2012).

As with environmental parameters, distribution of V_{rot} was compared by tornado rating and supercell class (Fig. 11), diurnal versus nocturnal (Fig. 12), and by radial bin from TC center (Fig. 13). Distributions of values were offset by more than a quartile higher for EF1+ tornado cases compared to EF0, consistent with the hypothesis of a positive correlation between EF scale and V_{rot} magnitude, but the EF0 supercell-only distribution overlapped considerably with all EF1+ events. Marginal supercells were lower by more than a quartile in their V_{rot} distributions compared to full supercells. V_{rot} trended higher at night than diurnally for the dataset as a whole, indicating some association with the stronger nocturnal measures of vertical shear (e.g., those in Fig. 8). However, no substantive distinction was evident between distributions of V_{rot} with distance from TC center, consistent with the substantial overlap in 0–6-km BWD distributions (Fig. 9b). With regard to radial distance, the relative statistical distribution patterns of V_{rot} matched those of 0–6-km BWD most closely among the various environmental parameters. V_{rot} also was compared against environmental variables and parameters for the dataset as a whole. All exhibited poor correlation in their scatter, the highest R^2 value arising from linear regression of V_{rot} with 0–6-km BWD (Fig. 14).

d. Echo tops

As with V_{rot} cases, ET distributions were determined with respect to tornado rating and supercell class (Fig. 15), day and night (Fig. 16) and in each 56-member subset of distance from TC center (Fig. 17). All heights for TDSs discussed herein are above radar level (ARL). The median echo top varied little across tornado and storm-mode categories, though the lower ≈1/3 of the distributions of EF0 (all) and marginal supercells yielded substantially lower echo tops than those segments of the EF1+ and supercellular events. ETs varied little between day and night, or between the inner 299 km of TCs and greater distances. The latter finding was antihypothetical, given the greater values of CAPE found in previous studies of radial buoyancy distributions (e.g., McCaul 1991). However, as noted in section 3b, measures of CAPE herein increased only slightly, if at all, in the outer sector, while indicators of shear increased inward, resulting in great overlap of distributions of bulk indices such as STP

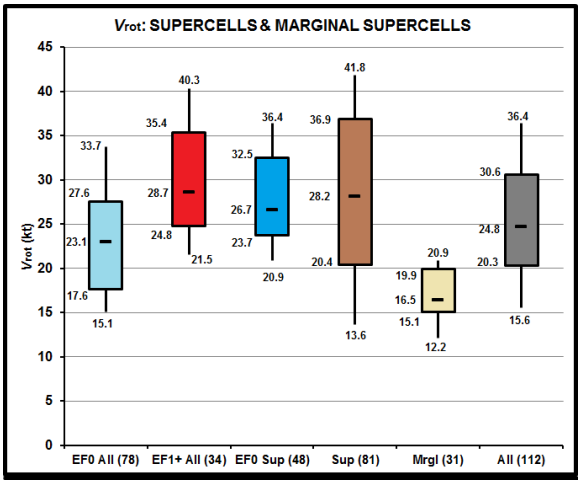

Figure 11: As in Fig. 4, but for V_{rot}.

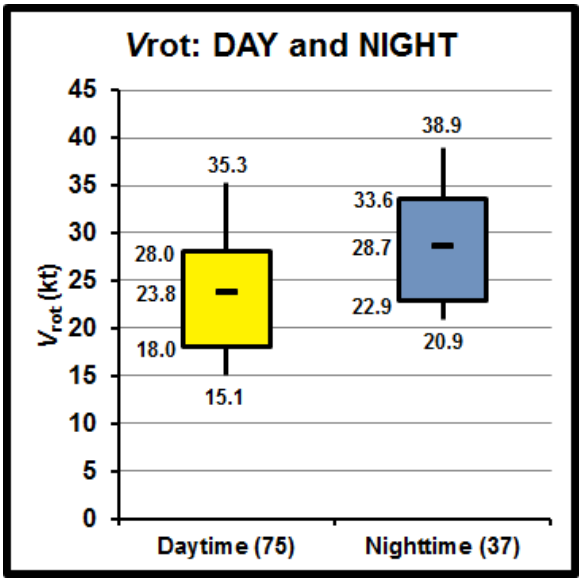

Figure 12: As in Fig. 6, but for V_{rot}.

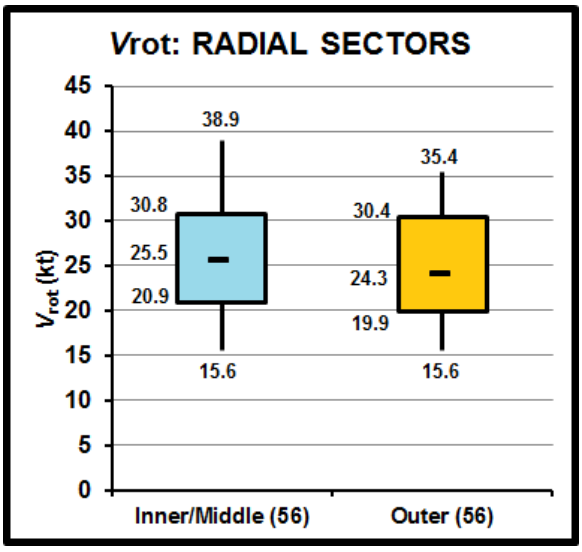

Figure 13: As in either panel of Fig. 9, but for V_{rot}.

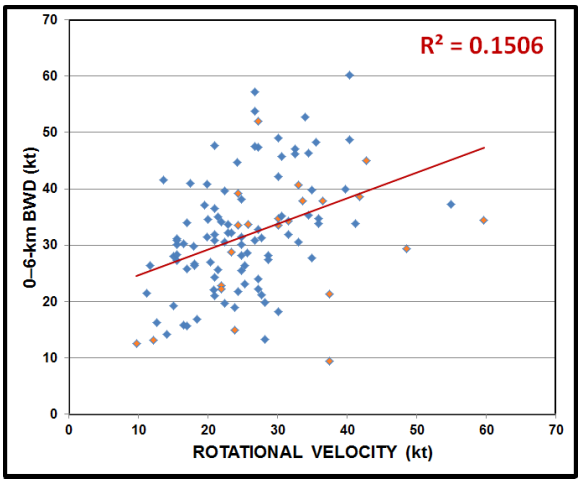

Figure 14: As in Fig. 10 but for V_{rot} and 0–6-km BWD. A linear regression is drawn (red) with coefficient of determination R^2 provided.

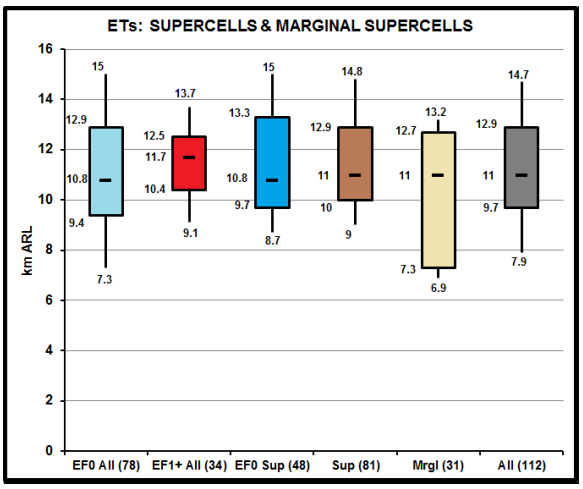

Figure 15: As in Fig. 4, but for ETs (km ARL).

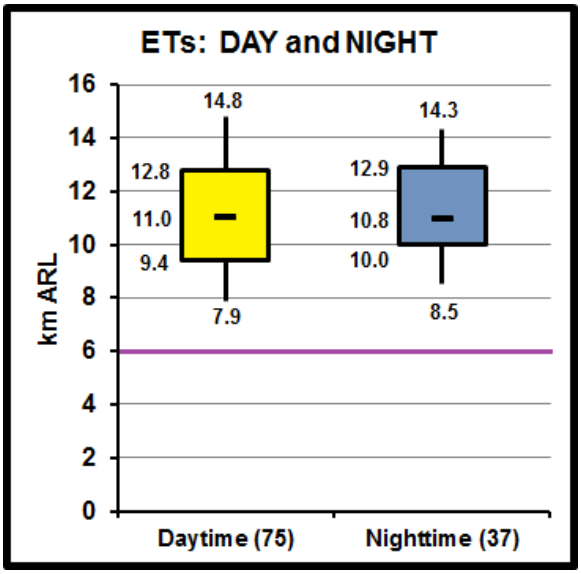

Figure 16: As in Fig. 6, but for ET (km ARL). Purple line approximates the 6-km AGL BWD level.

and SCP. That inner-outer counterbalancing of parameters contributing to supercell vigor indeed does appear consistent with no substantial change in ETs. When comparing ET against V_{rot} for the entire dataset, considerable scatter appeared (Fig. 18) and correlation was quite poor.

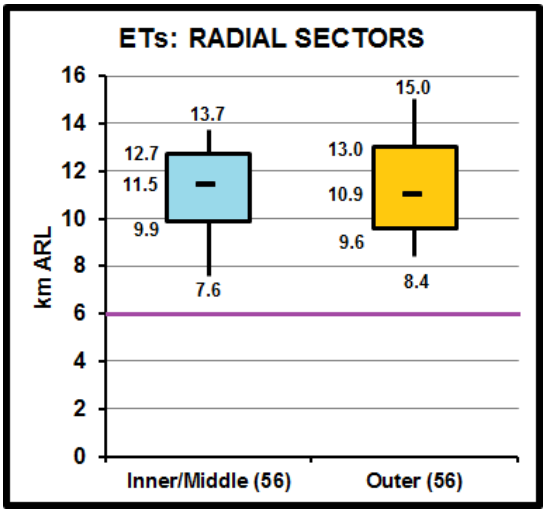

Figure 17: As in Fig. 15, but for radial sectors <200 km from TC center (cyan) and ≥200 km (gold).

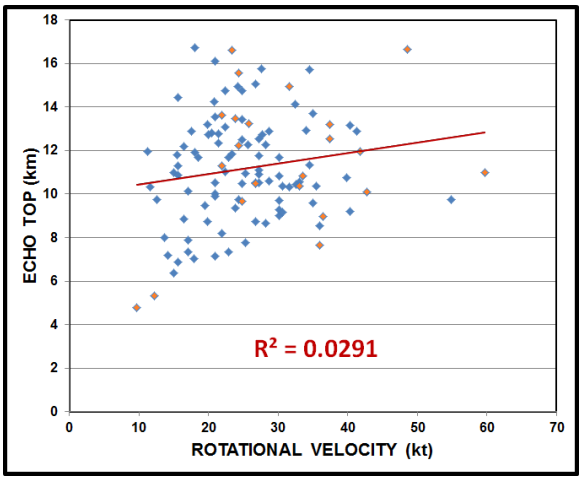

Figure 18: As in Fig. 14 but for V_{rot} and ET.

e. Tornadic debris signatures

A total of 23 events exhibited ρ_{hv} signatures consistent with a TDS, given the methods described and referenced in section 2. Because WSR-88D units were retrofitted with dual-polarimetric capabilities in temporally staggered fashion and part-way through the 2010–2014 examination period—instead of their being activated essentially at once—computing a percentage of our total cases containing a ρ_{hv} anomaly does not offer any meaningful insight into the true fraction of TC tornado reports associated with a TDS. A separate study is planned to investigate that issue and other aspects of all discoverable TC TDS events (not just those associated with filtered tornado segments). That effort also should optimize sample size for analysis.

Nonetheless, some preliminary TDS-related findings for the 23 cases can be offered here. As evident in Table 1, TDSs encompassed widely varying fractions of the echo depths, from 2% (lowest scan close to the radar with a 250-m TDS top) to 84% of a 6.4-km ET height. Another one-beam-depth TDS covered 3% of ET with a top of just 263 m. The deepest TDS in absolute terms was 9.2 km, reaching to 69% of the ET.

Table 1: Summary of TDS characteristics from the entire dataset: lowest columnar ρ_{hv} value, height ARL (m), percentage of associated ET, and V_{rot} (kt).

TDS	ρ_{hv}	Height (m)	% ET	V_{rot} (kt)
AVERAGE	.53	3533	23	30.7
MEDIAN	.50	2858	34	30.1
MAXIMUM	.895	9166	84	59.7
MINIMUM	.208	250	02	9.7

In terms of environmental characteristics within TDS cases, they generally did not stand out within the larger dataset. This applies to individual kinematic and thermodynamic parameters and for combinations of them (e.g., the bulk indices or the CAPE vs. SRH diagram in Fig. 10, note orange dots). TDS cases also were scattered throughout most of the distributions of V_{rot} cases, echo tops, and comparisons of each with assorted environmental parameters (e.g., the orange-colored members plotted in Figs. 14 and 18). Though small in number, this indicates that, to whatever extent a TDS may imply deeper storms, more favorable meteorological environments, or stronger storm-scale rotation, such influences are masked by other, unknown factors in the TC setting.

4. AVENUES for FURTHER EXAMINATION

The main limitation to more detailed and robust analyses (both statistically and categorically) is sampling. With a relative dearth of tornado-producing TCs in the period of super-resolution and especially dual-polarized radar data, the only solution is time and the occurrence of more events. Formal examination and presentation of the work presented here likely awaits a few more years of additional cases, acknowledging the high year-to-year variability in TC tornado occurrence (Edwards 2012).

As a separate issue, however, more intensive scrutiny and documentation just of TC TDS events can be done, and is planned. In examining TDSs for this study, we encountered others associated with tornadoes discarded by our filtering methods. We also encountered by happenstance a few well-defined ρ_{hv} anomalies strongly resembling tornadic cases, but not associated with any reports. Those also will be included in any future study specifically targeting the TC TDS phenomenon.

Given such a small sample size of TDSs herein, and the aforementioned complication in comparison with non-TDS cases, it is not possible yet to draw meaningful conclusions about the differences in environmental characteristics, ETs, or V_{rot}, or tornado intensity as implied by EF rating, between events with and without TDSs. To do so, additional comparisons will need to be made strictly using either: 1) aggregation of cases from the same local radars since each became dual-polarized at differing times, or 2) in bulk, starting at a single time when all radars in the dataset had acquired the capability. In particular, we hypothesize that TC TDS cases should have a greater damage rating, stronger V_{rot} and higher ET, compared to non-TDS tornado reports, Testing of these hypotheses also is planned, with larger sampling over a longer time span.

ACKNOWLEDGMENTS

We gratefully acknowledge Israel Jirak (SPC) for his astute manuscript review and suggestions. John Hart (SPC) wrote the radial-plotting script for Fig. 1b. Our analysis benefited from discussions with and questions from Howie Bluestein, Don Burgess, Bill McCaul and Joey Picca. The SPC Science Support Branch expertly maintains the environmental dataset and all software and hardware used for our analyses.

REFERENCES

Bodine, D. J., M. R. Kumjian, R. D. Palmer, P. L. Heinselman, and A. V. Ryzhkov, 2013: Tornado damage estimation using polarimetric radar. *Wea. Forecasting*, **28**, 139–158.

Bringi, V. N., and V. Chandrasekar, 2001: *Polarimetric Doppler Weather Radar: Principles and Applications*. Cambridge University Press, 636 pp.

Brown, R. A., V. T. Wood, and D. Sirmans, 2002: Improved tornado detection using simulated and actual WSR-88D data with enhanced resolution. *J. Atmos. Oceanic Technol.*, **19**, 1759–1771.

Brown, R. A., B. A. Flickinger, E. Forren, D. M. Schultz, D. Sirmans, P. L. Spencer, V. T. Wood, and C. L. Ziegler, 2005: Improved detection of severe storms using experimental fine-resolution WSR-88D measurements. *Wea. Forecasting*, **20**, 3–14.

Bunkers, M. J., B. A. Klimowski, J. W. Zeitler, R. L. Thompson, and M. L. Weisman, 2000: Predicting supercell motion using a new hodograph technique. *Wea. Forecasting*, **15**, 61–79.

Cifelli, R., S. W. Nesbitt, S. A. Rutledge, W. A. Petersen, and S. Yuter, 2007: Radar characteristics of precipitation features in the EPIC and TEPPS regions of the east Pacific. *Mon. Wea. Rev.*, **135**, 1576–1595.

Edwards, R., 2010: Tropical cyclone tornado records for the modernized National Weather Service era. Preprints, *25th Conf. on Severe Local Storms*, Denver, CO, Amer. Meteor. Soc., P2.7.

——, 2012: Tropical cyclone tornadoes: A review of knowledge in research and prediction. *Electronic J. Severe Storms Meteor.*, **7** (6), 1–61.

——, and A. E. Pietrycha, 2006: Archetypes for surface baroclinic boundaries influencing tropical cyclone tornado occurrence. Preprints, 23rd Conf. on Severe Local Storms, Saint Louis, MO, Amer. Meteor. Soc., P8.2.

——, A. R. Dean, R. L. Thompson and B. T. Smith, 2012a: Convective modes for significant severe thunderstorms in the contiguous United States. Part III: Tropical cyclone tornadoes. *Wea. Forecasting*, **27**, 1114–1135.

——, ——, ——, and ——, 2012b: Nonsupercell tropical cyclone tornadoes: Documentation, classification and uncertainties. Preprints, *26th Conf. on Severe Local Storms*, Nashville TN, Amer. Meteor. Soc., 9.6.

——, J. G. LaDue, J. T. Ferree, K. Scharfenberg, C. Maier, and W. L. Coulbourne, 2013: Tornado intensity estimation: Past, present, and future. *Bull. Amer. Meteor. Soc.*, **94**, 641–653.

Johns, R. H., and C. A. Doswell III, 1992: Severe local storms forecasting. *Wea. Forecasting*, **7**, 588–612.

Lakshmanan, V., K. Hondl, C. K. Potvin, and D. Priegnitz, 2013: An improved method for estimating radar echo-top height. *Wea. Forecasting*, **28**, 481-488.

McCaul, E. W. Jr., 1991: Buoyancy and shear characteristics of hurricane-tornado environments. *Mon. Wea. Rev.*, **119**, 1954–1978.

National Weather Service (NWS), 2010: Technical implementation notice 10-23. [Available online at http://www.roc.noaa.gov/WSR88D/PublicDocs/DualPol/tin_10-23dual_pol88d.pdf.]

NWS Warning Decision Training Branch, cited 2015: Dual-pol radar applications: Tornadic debris signatures. [Available online at http://www.wdtb.noaa.gov/courses/dualpol/Applications/TDS/player.html.]

Ryzhkov, A. V., T. J. Schuur, D. W. Burgess, and D. S. Zrnić, 2005: Polarimetric tornado detection. *J. Appl. Meteor.*, **44**, 557–570.

Spoden, P. J., R. A. Wolf, and L. R. Lemon, 2012: Operational uses of spectrum width. Electronic J. Severe Storms Meteor., 7 (2), 1–28.

Schneider, R. S., and A. R. Dean, 2008: A comprehensive 5-year severe storm environment climatology for the continental United States. Preprints, *24th Conf. on Severe Local Storms*, Savannah, GA, Amer. Meteor. Soc., 16A.4.

Schultz, L. A., and D. J. Cecil, 2009: Tropical cyclone tornadoes, 1950–2007. *Mon. Wea. Rev.*, **137**, 3471–3484.

Smith, B. T., R. L. Thompson, J. S. Grams, C. Broyles, and H. E. Brooks, 2012: Convective modes for significant severe thunderstorms in the contiguous United States. Part I: Storm classification and climatology. *Wea. Forecasting*, **27**, 1136–1153.

——, ——, and A. R. Dean, 2014: The Storm Prediction Center tornadic storm and environment database: Development and application. Preprints, *27th Conf. on Severe Local Storms*, Madison, WI, 17.1.

——, ——, ——, and P. T. Marsh, 2015: Diagnosing the conditional probability of tornado damage rating using environmental and radar attributes. *Wea. Forecasting*, **30**, 914–932.

Thompson, R. L., B. T. Smith, J. S. Grams, A. R. Dean, and C. Broyles, 2012: Convective modes for significant severe thunderstorms in the contiguous United States. Part II: Supercell and QLCS tornado environments. *Wea. Forecasting*, **27**, 1136–1154.

Torres, S. M., and C. D. Curtis, 2007: Initial implementation of super-resolution data on the NEXRAD network. Preprints, *23rd Conf. on International Interactive Information and Processing Systems (IIPS) for Meteorology, Oceanography, and Hydrology*, San Antonio, TX, Amer. Meteor. Soc., 5B.10.

WSEC, 2004: A recommendation for an enhanced Fujita scale (EF-scale). Wind Science and Engineering Center, Texas Tech University, 95 pp. [Available online at http://www.spc.noaa.gov/faq/tornado/ef-ttu.pdf.]